ADAPTIVE FREE BOUNDARY APPROACH TO SIMULATE LIQUID FLOW IN MICRO CHANNELS WITH SLIP BOUNDARY CONDITIONS

Raman Balu[†]**, Selvakumar Ulaganathan**[*]

[†]Dean, School of Mechanical Engineering,
Noorul Islam Centre for Higher Education, India.
e-mail: balshyam2003@yahoo.com

[*]Graduate student, Dept. of Aerospace Sciences,
Cranfield University, United Kingdom.
e-mail: ulag.selva@gmail.com

ABSTRACT

Phenomenal advances in the computational fluid dynamics, over the past few decades, have revolutionised and greatly benefited areas like bio-medicine, where accurate flow simulation leads to new and better insight into the surgical procedures and of optimum design of modern medical gadgets. In this paper, a free floating boundary approach is used to solve the conventional laminar compressible boundary layer equations, which simulate the flow of a viscous liquid in very small channels, using an efficient implicit finite difference scheme called the Keller's box scheme, with appropriate slip boundary conditions at the wall. This approach leads to very accurate solutions and the estimation of wall shear stress and heat transfer distribution along the length of the channel. These are useful in the design of micro devices like Lab-on-Chip drug delivery system and blood flow simulation through heart and veins and many other applications where the slip flow assumption is reasonably valid.

Keywords: Blood flow simulation, laminar flow with wall slip, Keller's Box scheme, Nonlinear boundary-value problems, Free boundary formulation.

1 Introduction

Recent developments in the computational fluid dynamic simulations have a profound and beneficial impact on several other disciplines like medicine and biology, besides aeronautical and aerospace applications. For example, the conventional methods of surgery and treatment have given way to the most sophisticated modern procedures using the latest available computer simulation tools. It is well known that cardiovascular disease is the major cause of a large number of deaths in the present day world [1]. The understanding, diagnosis and treatment of the disease heavily relies on the study and analysis of cerebral blood flow behavior. Major problems are traced to the anomalous blood flow pattern in the neighborhood of critical bifurcations within the brain leading to strokes for instance. Experimental studies are often impractical in such situations. Data, both static and dynamic are normally acquired by computer tomography (CT) or three dimensional rotational angiography (3DRA). Not withstanding these useful practical technologies in measurements, modeling and flow simulations are now playing a major role in the proper administration of the treatment procedures. The limitations that are inherent in experimental techniques, are, to a large extent complemented by flow simulations. Nowadays entire brain neurovasculature blood flow simulations are possible which ably supports the clinical neurosurgery. This capability offers the clinician the possibility of performing non-invasive, patient specific simulations experiments in a virtual mode and in real time. This helps to study and analyse in advance

the effect of a particular or alternative course of surgical procedures with no implied danger or risk to the patient. This also gives support for diagnosis and therapy. Simulations also offer the unique prospects of gaining useful insights into the poorly understood blood flow patterns even in the normal brain. Figure 1 shows a real time system for blood flow analysis consisting of MRI, CT, X-ray data acquisition, creation of 3D model and interactive flow visualisation.

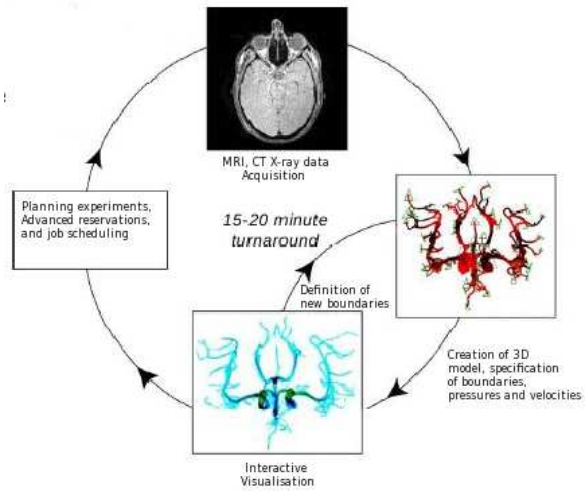

Figure 1: System for real time anlysis of blood flow.

Conventional three dimensional Computational Fluid Dynamics codes, which basically rely on continuum flow assumption, solve the basic governing equations (Navier - Stokes) by numerical techniques like finite element, finite volume and finite difference methods with appropriate boundary conditions for the given flow geometry. The shear stresses and pressure distributions are calculated from the flow velocity and temperature fields, which are obtained as part of the solution. For complex applications like blood flow mapping, there is a need to utilize scalable high performance parallel computing systems running on Linux operating systems, to get the simulation results in near real time mode. To overcome these limitations of super computer class resource requirements, there is a need to use less sophisticated flow models without sacrificing the accuracy. In this context highly accurate solutions with boundary layer assumptions and appropriate wall velocity and temperature slip boundary conditions can be often used. In cases where the continuum flow assumptions breaks down, free molecular approach using Lattice - Boltzmann method is used, which also requires the super computing systems.

2 Formulation of the Problem

2.1 Governing Equations

The conventional two dimensional, laminar, compressible boundary layer fluid flow under slip conditions at low Mach numbers is considered. It is governed by the following fundamental boundary layer equations.

$$\frac{\partial u}{\partial x} + \frac{\partial v}{\partial y} = 0 \tag{1}$$

$$u\frac{\partial u}{\partial x} + v\frac{\partial u}{\partial y} + \frac{1}{\rho}\frac{dP(x)}{dx} = \nu\frac{\partial^2 u}{\partial y^2} \tag{2}$$

$$u\frac{\partial T}{\partial x} + v\frac{\partial T}{\partial y} = \frac{\alpha}{\rho c_p}\frac{\partial^2 T}{\partial y^2} \tag{3}$$

where P, T, ρ, ν, α, and c_p refer to the pressure, temperature, density, kinematic viscosity, thermal diffusivity and specific heat, respectively. The positive x-coordinate is measured along the surface and the positive y-coordinate is measured normal to the x-axis in the outward direction towards the fluid. The velocity components along the x-axis and y-axis are u and v respectively. The velocity gradients in the x-direction are small compared to velocity gradients in the y-direction.

2.2 Slip Effects

For nearly over a hundred years, scientists and engineers have applied the classical *no-slip* boundary condition, for fluid flow over a solid surface. While this condition has been validated experimentally for a number of macroscopic flows, it still remains an *assumption* and is not based on sound physical reasoning. In fact two hundred years ago, Navier himself proposed, a more general boundary condition which includes the possibility of fluid slip at a solid surface. He proposed that at the solid boundary the velocity is proportional to the shear rate at the surface,

$$u_{fluid} = \lambda \left(\frac{du}{dy}\right)_s \tag{4}$$

where u_{fluid} is the fluid velocity at the solid surface and λ refers to the *slip coefficient* having a length scale as illustrated in Figure 2. In this equation λ can be interpreted as fictitious length below the surface, at which the normal slip boundary conditions apply. For conventional *no-slip* condition $\lambda = 0$. If λ is finite, its effect depends on the scale of the flow.

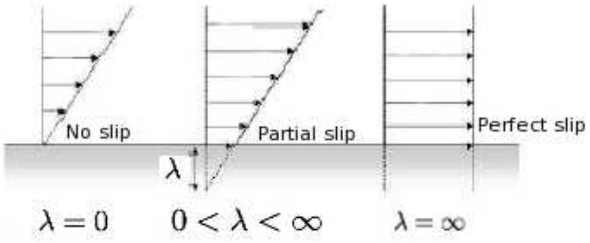

Figure 2: Generalised slip flow boundary condition at a solid surface

2.3 Transformed Equations

Analysis of the flow is simplified by using the following boundary layer coordinate η and non-dimensional stream function f. [2]

$$\eta = y\sqrt{\frac{u_\infty}{\nu x}} \tag{5}$$

$$f = \frac{\Psi}{\sqrt{\nu x u_\infty}} \tag{6}$$

A governing equation for the non-dimensional stream function f can be found by substituting these non-dimensional terms into the x-momentum equation (2):

$$f''' + 0.5ff'' = 0 \tag{7}$$

The slip boundary conditions are,

$$f(\eta = 0) = 0 \tag{8}$$

$$f^{'}(\eta = 0) = K1 f^{''}(0) \tag{9}$$

where $K1$ is the slip coefficient, which is introduced by rewriting equation (4), defined for liquids by:

$$K1 = \left(\frac{\lambda}{x}\right)(Re_x)^{1/2} \tag{10}$$

$$f^{'}(\eta \to \infty) = 1 \tag{11}$$

The temperature in the equation (3) is non-dimensionalised as,

$$\theta = \frac{T - T_w}{T_\infty - T_w} \tag{12}$$

where T_∞ is the free stream temperature and T_w is the surface temperature.
Using the non-dimensionalisation used for the fluid flow equations, and the non-dimensional temperature, the heat equation becomes:

$$\theta^{''} + 0.5Pr\left(\theta^{'} f - \theta f^{'}\right) = 0 \tag{13}$$

where Pr is the Prandtl number of the liquid. The boundary condition is,

$$\theta(\eta = \infty) = 1 \tag{14}$$

For the case of constant heat flux, the non-dimensional temperature becomes [3],

$$\theta(\eta) = \frac{T - T_\infty}{(q_w^{''} x / k_\infty)} Re^{1/2} \tag{15}$$

with associated boundary conditions:

$$\theta^{'}(\eta = 0) = -1 \tag{16}$$

$$\theta(\eta = \infty) = 0 \tag{17}$$

3 The Free Boundary Approach

Boundary value problems on infinite intervals $(-\infty, \infty)$ arise in several branches of science and engineering. A classical numerical approach of these problems is to replace the original problem by the one defined on a finite interval, say $[a, x_\infty]$, where a is the truncated boundary corresponding to $-\infty$ and x_∞ is a truncated boundary corresponding to ∞ [4]. Assuming a is finite, the original problem is solved by comparing the numerical results obtained for several values of x_∞. The value of x_∞ is varied until the computed results stabilize, at least, to a preferred number of significant digits. However, a truncated boundary allowing for a satisfactory accuracy of the numerical solution has to be determined by the trial and error, and this seems to be the major drawback of the classical approach. In order to overcome this difficulty, a different approach is formulated, in which the free boundary or the truncated boundary is treated as an unknown variable and is determined as part of the solution. This eliminates the uncertainty related to the choice of the truncated boundary in the classical treatment of boundary value problems defined on infinite intervals.

The general boundary value problem on an infinite interval is defined as,

$$\frac{d\mathbf{y}}{dx} = \mathbf{f}(x, \mathbf{y}), \qquad x \in [a, \infty] \tag{18}$$

with the associated boundary conditions:

$$\mathbf{g}(\mathbf{y}(a), \mathbf{y}(\infty)) = \mathbf{0} \tag{19}$$

where $\mathbf{y}(x)$ is a n-dimensional vector with $\mathbf{y}_l(x)$ for $l = 1, \ldots, n$ as components and a, ∞ are the lower and upper boundaries respectively. If a is a finite value, then it denotes that the boundary value problem is defined on an semi-infinite interval. Since we are introducing an upper boundary as a variable, it is necessary to introduce one more boundary condition. We assume that the additional boundary condition is available as,

$$h(\mathbf{y}(a), \mathbf{y}(\infty)) = 0 \tag{20}$$

Then the free boundary formulation of equation (18),(19) and (20) is given as,

$$\frac{d\mathbf{y}}{dx} = \mathbf{f}(x, \mathbf{y}), \qquad x \in [a, x_\varepsilon] \tag{21}$$

$$\mathbf{g}(\mathbf{y}(a; \varepsilon),\ \mathbf{y}(x_\varepsilon; \varepsilon)) = \mathbf{0} \tag{22}$$

$$h(\mathbf{y}(a; \varepsilon),\ \mathbf{y}(x_\varepsilon; \varepsilon)) = \varepsilon \tag{23}$$

where $0 < |\varepsilon| \ll 1$, the solution of equation (21) depends on ε, that is $\mathbf{y}(x; \varepsilon)$. Here $\mathbf{y}(x; \varepsilon)$ is an approximation to $\mathbf{y}(x)$ on $[a, x_\epsilon]$, and x_ε is unknown. If we set $\varepsilon = 0$, then $(\mathbf{y}(x), \infty)$ is a solution of equation (21). Each solution $\mathbf{y}(x)$ of equation (18) and $\mathbf{y}(x; \varepsilon)$ of equation (20) are *isolated* at least in a neighborhood of $\varepsilon = 0$. Furthermore, x_ε is a differentiable function of ε on a neighborhood $\mathbf{I}_o$ of $\varepsilon = 0$ and that the limit of $\mathbf{d}x_\varepsilon/\mathbf{d}\varepsilon$ as ε goes to zero exists. If all the components of $\mathbf{y}(x; \varepsilon)$ and of $(d\mathbf{y}/d\varepsilon)(x; \varepsilon)$ are continuous functions on the domain $[a, x_\varepsilon] \times \mathbf{I}_o$, then the solution of equation (20) converges uniformly to the solution of equation (18), as ε tends to zero.

Using x_∞ as the $(n+1)^{th}$ component of the vector $\mathbf{y}$. (i.e).$y_{n+1} = x_\varepsilon$, a new independent variable is defined as follows to map the region $[a, x_\infty]$ into [0,1],

$$z = \frac{(\eta - a)}{(y_{n+1} - a)} \tag{24}$$

Then the original boundary value problem given by equation (18) is now transformed to,

$$\frac{d\mathbf{Y}}{dz} = \mathbf{F}(z, \mathbf{Y}), \qquad z \in [0, 1] \tag{25}$$

with the associated boundary condition:

$$\mathbf{G}(\mathbf{Y}(0),\ \mathbf{Y}(1)) = 0 \tag{26}$$

where we have defined

$$\mathbf{Y}(z) \equiv (\mathbf{y}(z),\ y_{n+1})^T \tag{27}$$

$$\mathbf{F}(z, \mathbf{Y}) \equiv ((y_{n+1} - a)\mathbf{f}((y_{n+1} - a)z + a, \mathbf{y}),\ 0)^T \tag{28}$$

$$\mathbf{G}(\mathbf{Y}(0), \mathbf{Y}(1)) \equiv (\mathbf{g}(\mathbf{y}(0), \mathbf{y}(1)), h(\mathbf{y}(0), \mathbf{y}(1)) - \varepsilon)^T \tag{29}$$

4 Keller's Box Scheme

In the present work, an efficient implicit finite difference method, called the Keller's box scheme, originally developed by Keller, has been applied to solve equations (7) and (13) subject to the boundary conditions (8),(9),(11) and (14). The system of equations (7) and (13) is reduced to a system of first-order equations by defining new variables:

$$f^{'} = u\eta_{\infty} \tag{30}$$

$$u^{'} = v\eta_{\infty} \tag{31}$$

$$v^{'} = -fv\eta_{\infty} \tag{32}$$

$$\theta^{'} = \theta_1\eta_{\infty} \tag{33}$$

$$\theta_1^{'} = -Prf\theta_1\eta_{\infty} \tag{34}$$

$$\eta_{\infty}^{'} = 0 \tag{35}$$

Equations (30)-(35) can be put in the following general form.

$$\mathbf{Q}_i^{'} = \mathbf{G}_i(f, u, v, \theta, \theta_1, \eta_{\infty}); \quad i = 1, 2, ..., 6 \tag{36}$$

where $\mathbf{Q}$ is defined as,

$$\mathbf{Q} = \mathbf{Q}(f, u, v, \theta, \theta_1, \eta_{\infty}) \tag{37}$$

The boundary conditions (8),(9),(11) and (14) can also be put in the general form as follows.

$$\mathbf{Q}_i(0) = \mathbf{C}_i \tag{38}$$

where i=1,2,4 for a prescribed wall temperature case and i=1,2,5 for a prescribed wall heat flux case.

$$\mathbf{Q}_{i_m}(\eta_{\infty}) = \mathbf{C}_{i_m} \tag{39}$$

where m=1,2,3 such that $i_1 = 2$, $i_2 = 3$, $i_3 = 4$. The additional boundary condition which is imposed is that v becomes within ϵ (ideally zero) at the boundary layer edge. Here the boundary conditions at η_{∞} are written with a subscript i_m, in order that the variables specified at $\eta = 0$ and $\eta = \eta_{\infty}$ may not be disjoint. The region 0 to η_{∞} is now divided into $(\mathbf{J} - 1)$ steps. The step size for equal spacing is given by,

$$\mathbf{\Delta}\eta = \eta_{\infty}/(\mathbf{J} - 1) \tag{40}$$

where $\mathbf{J}$ is the number of grid points in the basic net. On the net chosen as above, let us define

$$\eta_{j+1/2} = \frac{1}{2}(\eta_j + \eta_{j+1}) \tag{41}$$

and for any general net function $\mathbf{G}_i$,

$$\mathbf{G}_i^{j+1/2} = \frac{1}{2}(\mathbf{G}_i^j + \mathbf{G}_i^{j+1}) \tag{42}$$

Differencing equation (36) at $\eta_{j+1/2}$, we get,

$$\mathbf{Q}_i^{j+1} - \mathbf{Q}_i^j = \frac{\mathbf{\Delta}\eta}{2}(\mathbf{G}_i^j + \mathbf{G}_i^{j+1}) \tag{43}$$

The differencing is done at the cell centre $(j+1/2)$ so that the finite differencing scheme retains second order accuracy even on non-uniform grids. We write for q^{th} iteration

$$\mathbf{Q}_i^{j(q+1)} = \mathbf{Q}_i^{j(q)} + \delta\mathbf{Q}_i^{j(q)} \tag{44}$$

and insert in equation (43) and neglecting higher order $\delta\mathbf{Q}_i^{j(q)}$:

$$\delta\mathbf{Q}_i^{(j+1)(q)} - \delta\mathbf{Q}_i^{j(q)} - \frac{\mathbf{\Delta}\eta}{2}(\mathbf{G}_i^{j(q)} + \mathbf{G}_i^{(j+1)(q)}) = \mathbf{F}_i^{j(q)}; \quad i = 1, 2, \ldots, 6$$
$$j = 1, 2, \ldots, \mathbf{J}$$
$$q = 0, 1, 2 \ldots \tag{45}$$

where

$$\mathbf{F}_i^{j(q)} = -\left(\mathbf{Q}_i^{(j+1)(q)} - \mathbf{Q}_i^{j(q)}\right) + \frac{\mathbf{\Delta}\eta}{2}(\mathbf{G}_i^{j(q)} + \mathbf{G}_i^{(j+1)q})$$
$$-\frac{\mathbf{\Delta}\eta}{2}\left(\sum_{i=1}^{n}\frac{\partial G}{\partial Q}|_i^{(j+1)(q)}\delta Q_i^{(j+1)(q)} + \sum_{i=1}^{n}\frac{\partial G}{\partial Q}|_i^{j(q)}\delta Q_i^{j(q)}\right) \tag{46}$$

Let us define the vectors

$$\delta\mathbf{Q}_j = (\delta f, \delta u, \delta v, \delta\theta, \delta\theta_1, \delta\eta_\infty) \tag{47}$$

where $\delta\mathbf{Q}_j$ is the increment vector. Now the equation (45) can be put in the following form.

$$\mathbf{R}_j\delta\mathbf{Q}_j - \mathbf{S}_j\delta\mathbf{Q}_j = \mathbf{P}_j \tag{48}$$

where,

$$\mathbf{P}_j = (\mathbf{F}_1, \mathbf{F}_2, \ldots, \mathbf{F}_6)_j \tag{49}$$

It may be observed that equation (45) for the increment vector ($\delta\mathbf{Q_j}$) is linear even though the governing equations are non linear. This can be solved by putting the equation (48) in the block tridiagonal form $A = LU$ and solved by Thomas algorithm [5]. Thus the increment vector $\delta\mathbf{Q}_j$ having the increments of all the variables, equation (47), is determined provided the initial profiles of all the variables are specified. It is to be noted that these profiles are to be consistent with the known boundary conditions. The increment is then added to the initial solution. The process is repeated until the maximum value of the incremental vector $|\delta\mathbf{Q}_j|$ is less than a prescribed tolerance, (say 10^{-6}). Provided that the initial profiles are close to the true solution, the above iterative process is quadratically convergent and unconditionally stable on arbitrary nets. In the present case, to initiate the process, initial guesses for the velocity and thermal fields were taken as linear profiles with $\eta_\infty = 4$. Thus

$$f = \eta^2/2\eta_\infty \tag{50}$$
$$f^{'} = \eta/\eta_\infty \tag{51}$$
$$f^{''} = 0.1 \tag{52}$$
$$\theta = f^{'} \tag{53}$$
$$\theta^{'} = f^{''} \tag{54}$$

The extra boundary condition that is needed for this method of solution is taken as shear stress at the boundary layer edge.

$$|v(\eta_\infty)| = |f^{''}(\eta_\infty)| = \epsilon \tag{55}$$

5 Results and Discussions

The free boundary technique has been used to solve the equations (1)-(3) for various values of **K1** and Pr. The location of the free boundary (boundary layer edge) in all the cases has been found automatically by the solution procedure as part of the solution depending on a prescribed accuracy 'ϵ'. The present results are compared with values obtained in ref [3] by Yazdi et al.

Figure 3 and 4 show the non-dimensional velocity at the wall as a function of **K1** for $Pr = 1.0$. The agreement with results of ref [3] is good. For **K1**= 0 the classical Blasius value of 0.332 is obtained for the wall shear. Results of ref [3] indicate this value as 0.322 obtained by shooting method with a fixed value (η_∞) of 5. This clearly demonstrates the superiority of the free boundary technique. From section (2.2), we observed that the zero slip coefficient corresponds to the no slip condition. Consequently, the velocity at the wall must be equal to zero. It is clear from the figure 3 that the non-dimensional wall velocity becomes zero as the slip coefficient approaches the value of zero. It is also clear that as the slip coefficient increases from zero, the fluid velocity increases at the wall.

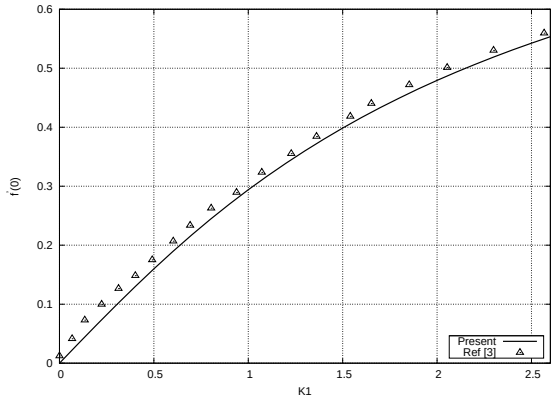

Figure 3: Non-dimensional wall velocity as a function of **K1**.

Figures 5 and 6 show the variation of velocity and shear stress in the boundary layer as a function of η. These profiles also show good agreement and correct trends. Figure 7 and 8 show the variation of wall temperature and Nu as a function of **K1**. It is observed that the non-dimensional slip coefficient increases the heat flux. The Nu number obtained presently show considerable variations with those obtained by shooting method of ref [3]. Figure 9 shows that value of η_∞ as a function of ϵ. It demonstrates the fact that as the accuracy is tightened (smaller ϵ) the value of η_∞ increase asymptotically. So when the value of η_∞ is fixed, it is difficult to get more accurate results if the value of η_∞ is less than the value which is required to maintain a small value of ϵ. This explains the fact behind the value of 0.322 which is obtained instead of 0.332 when the value of η_∞ is fixed as 5 in ref [3].

As per the boundary condition $f^{'}(0) = K1 f^{''}(0)$ and the present method satisfies this exactly over the entire range of $K1$ studied. This is illustrated in the figure (10), which shows a plot of $f^{'}(0)/f^{''}(0)$ .vs. $K1$ which should ideally be a straight line. In contrast, the results of Ref [3], does not corroborate this except for smaller values of $K1$ and that too only approximately. Thus the free adaptive boundary technique is seen to be more robust.

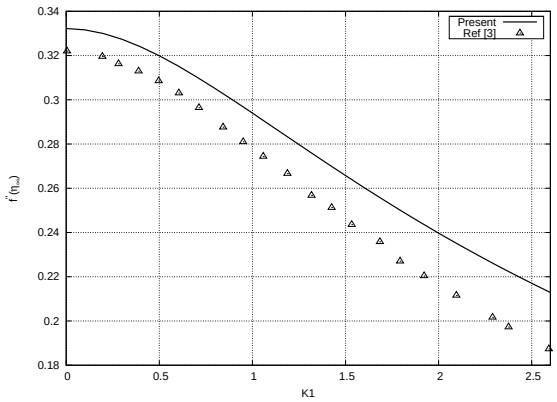

Figure 4: Non-dimensional wall shear stress as a function of **K1**.

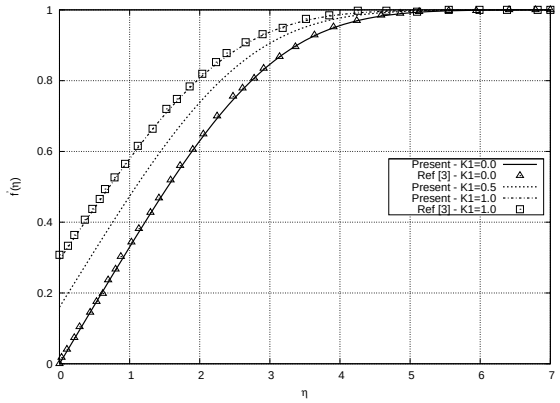

Figure 5: Non-dimensional velocity as a function of η.

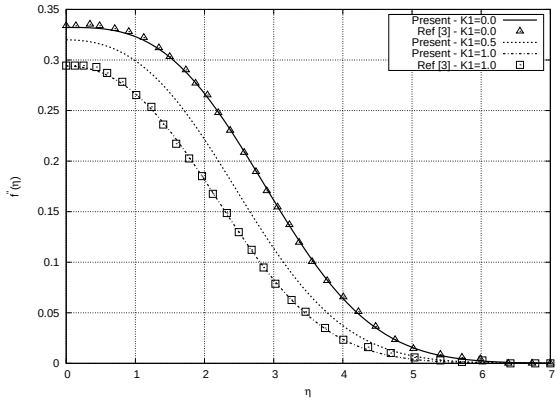

Figure 6: Non-dimensional shear stress as a function of η.

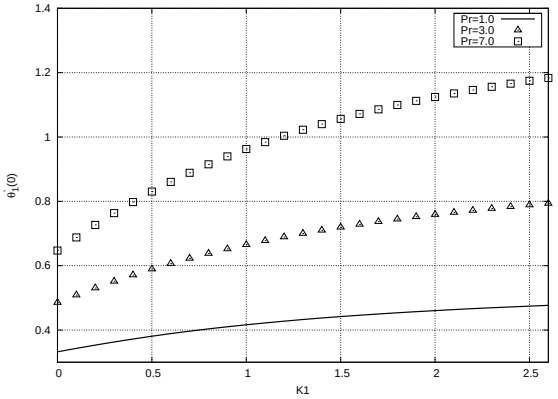

Figure 7: Non-dimensional wall heat flux as a function of **K1**.

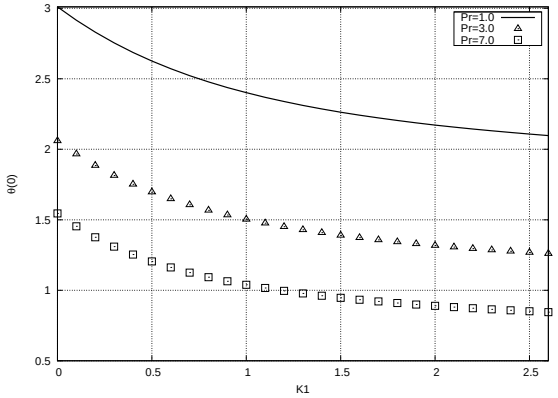

Figure 8: Non-dimensional wall temperature as a function of **K1**.

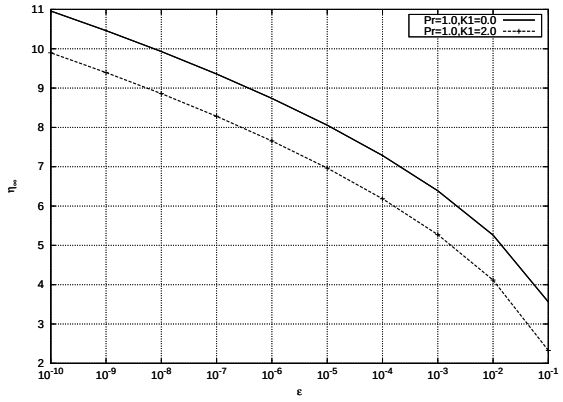

Figure 9: Free boundary as a function of ϵ.

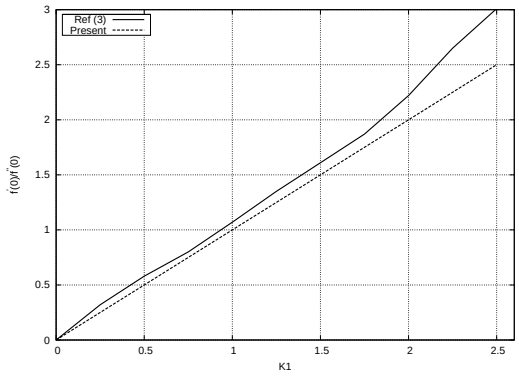

Figure 10: $f^{'}(0)/f^{''}(0)$ as a function of $K1$

6 Conclusions

A new free floating boundary approach is used to solve the conventional laminar compressible boundary layer equations. This approach solves the flow of viscous liquids in micro channels, using an efficient implicit finite difference scheme called the Keller's box scheme, with appropriate slip boundary conditions applied at the wall. Since the free boundary approach obtains the truncated boundary as part of the solution, it eliminates the uncertainty associated with the choice of the free boundary in solving the boundary value problems defined on infinite intervals. The obtained results show that an increase in slip coefficient tends to increase the fluid velocity and reduce the wall shear stress. It is also observed that the reduction of velocity gradient leads to the reduction of boundary layer thickness with the increase in slip coefficient. The heat flux and local Nusselt number are observed to have an increased value as the slip coefficient and Prandtl number tend to have a higher value. It is also observed that the wall temperature is reduced by the increase of slip coefficient and Prandtl number. It is seen that increase in accuracy levels increases the location of the infinite boundary asymptotically as expected. This approach enables less sophisticated models to be used for getting accurate solutions in practical applications where near real time simulations are needed.

References

[1] Zasada, S. & Coveney, P., Computational biomedicine: The role of workflow tools. *International Conference on Computational Sciences, ICCS 2010*, 2010.

[2] Martin, M.J. & Boyd, I.D., Stagnation-point heat transfer near the continuum limit. *Technical notes, AIAA Journal, Vol 47, No1*, pp. 283–285.

[3] M H Yazdi, I.H.A.Z., S Abdullah & Sopian, K., Friction and heat transfer in slip flow boundary layer at constant heat flux boundary conditions. *Mathematical methods, computational techniques, non-linear systems, intelligent systems, ISBN:978-960-474-012-3*, pp. 207–213, 1990.

[4] Fazio, R., A free boundary approach and keller's box scheme for bvps on infinite intervals. *International journal of computer mathematics, Vol80, No12*, pp. 1549–1560, 2003.

[5] Balu, R., An application of keller's method to the solution of an eigth-order nonlinear boundary value problem. *Int journal for numerical methods in engineering, Vol15*, pp. 1177–1186, 1980.